environment were large enough to cause a transition to another equilibrium state where a new mechanical balance within the stress fiber is needed to keep the structure, the cells may adapt to the environment by modulating their molecular compositions just as is done by the recruitment of α-smooth muscle actin. Stress fibers under isometric contraction are actually accompanied by rapid molecular exchanges of α-actinin and myosin with the ones in the surrounding cytoplasm [49]. Mechanical stimuli-induced deviations from an equilibrium state (or a homeostatic state) associated with the apparently static but actually dynamic isometric conditions (such as alterations in stress) may thus cause the mechanosensitive responses of stress fibers.

Why, then, is stress or strain kept constant instead of force? Actin filaments are bundled in parallel by α-actinin and myosin to form stress fibers, and the bundling is strengthened at the periphery of stress fibers where the cross-linking (with structural proteins talin and vinculin [3,15]) is rich in quantity and quality [49,61]. Focal adhesions as a mechanosensitive element [15,25,53] might be thus affected by stress having an interaction surface (because all of the paralleled actin filaments probably deform the focal adhesions together) rather than by force unrelated to cross-sectional area. Meanwhile, stress and strain are a concept of continuum mechanics to be exact. Considering the individual molecules, stress fibers having higher-order structures are not uniform materials. Each mechanosensitive element within stress fibers, such as α-smooth muscle actin [16] might sense tensional force or elongation (or force-induced conformational change that exposes cryptic binding or phosphorylation sites) in respective actin filaments or their associated proteins rather than the stress or strain detected at the whole stress fiber scale. As for mechanosensitive elements responsible for the stress fiber disassembly, one of the potential candidates is cofilin, which colocalizes with actin and conducts severing and possibly depolymerization [46,54]. These actin-associated proteins might be regulated by tensions in each actin filament as well.

4. Biomechanical properties in the cytoplasm

Soft substrates made by microfabrication have allowed quantification of the magnitude of isometric tension in stress fibers [57]. These measurements have demonstrated that tensions of the order of $\sim$1–40 nN in magnitude, depending on the size of large focal adhesions, are exerted on the substrate in smooth muscle cells. Single actin filaments *in vitro* are able to bear $\sim$600 pN at the maximum [58]. Forces generated by single myosin heads along actin filaments are on the order of $\sim$1–10 pN [32]. However, it remains unclear how tensions are borne and transmitted within stress fibers under isometric contraction. From modeling approach, force balances in one sarcomeric unit in stress fibers have recently been discussed by considering another structural protein, titin, similar to the titin or connectin that works as an elastic element in striated muscle [4,55]. Force balances on a scale that includes interactions between stress fibers and focal adhesions were also reported, focusing on Rho-kinase-mediated spatially different contractions of actomyosin [2]. Force balance in stress fibers and its role in various macroscopic mechanical behaviors were also discussed from a tensegrity approach [41].

The lack of our knowledge about the force balance and transmission within stress fibers is partly because the mechanical properties of stress fibers were unclear. Recently, however, there have been increasing data on them. Kumar et al. [35] evaluated viscoelastic properties of stress fibers in living endothelial cells from their retraction behavior seen after being severed by laser cutting. The retraction was slowed or virtually abolished by inhibition of Rho-kinase or calmodulin/MLCK, respectively. Lu et al. [40] measured transverse (perpendicular to the longitudinal length) elastic modulus of individual stress fibers in living endothelial cells by indentation using an atomic force microscope. They revealed

that the elastic modulus of stress fibers, in which the contractile level was decreased with blebbistatin, was smaller than those in which the contractile level was increased with calyculin A. The elastic modulus was in the range of ~10 kPa, whereas the smallest values reported by Deguchi et al. [8,10] on stress fibers isolated from cells was ~300 kPa. One major difference between Lu's and Deguchi's experiments is that the former measured a transverse elastic modulus based on a small indentation depth of 200 nm while the cells were subjected to unidirectional stretch of ~8%; meanwhile, the latter measured a longitudinal elastic modulus based on ~20% axial stretch. As the stress fiber is undoubtedly an anisotropic material in which filamentous structures are bundled more or less in parallel, it seems reasonable to have elastic modulus of such different magnitudes depending on the loading direction.

Focusing on the same stress fibers inside cells, Lu's data demonstrated that the elastic modulus after the contractile level was increased was larger in the peripheral regions than that in the central regions [40]. This heterogeneous distribution of the elastic modulus along the long axis of individual stress fibers may be comparable to the non-uniform deformation of stress fibers, reported by Peterson et al. [49] after enhancement of contraction by calyculin A. They demonstrated that peripheral stress fibers shortened in length, whereas central ones were elongated probably due to passive stretching caused by stronger peripheral contraction. We touch on this topic more in detail in the following section.

5. Non-uniform contraction behavior

Why is the non-uniform deformation generated in the same stress fibers, even though they have periodic and hence regular sarcomeric structures along the long axis in non-motile cells? This still remains unclear; however, the origin has been discussed from various modeling approaches. Besser and Schwarz [2] assumed that Rho-kinase that phosphorylates MLC is rich in concentration around the cell periphery, thereby leading to higher stress fiber contraction at the periphery compared to the central region. This assumption came from ideas that the guanine nucleotide exchange factor for RhoA is activated at focal adhesions; and then activated GTP-bound Rho, the upstream signal of Rho-kinase, becomes richer in concentration near the focal adhesions rather than the central region. The spatial difference in Rho-kinase concentration is, however, still controversial as RhoA and Rho-kinase were reported to exist along the stress fibers [28]. Moreover, the myosin-binding subunit of myosin phosphatase (phosphorylated by Rho-kinase to inhibit the activity of this enzyme and to activate MLC accordingly) was also associated with stress fibers [24,42]. To account for the non-uniform deformation, other modeling studies [41,55] assumed a parameter by which the contractile force becomes stronger near the periphery than the central region. The phosphorylation level of MLC is indeed higher around the periphery than the central region [49,61], which may support this assumption.

Nevertheless, no mechanism has yet appeared that describes why MLC should be higher in concentration and be activated more at the peripheral region of stress fibers than the central region. The stress fiber assembly process (of motile cells) basically consists of mDia-based elongations and subsequent connections with different actin bundles followed by their actomyosin contraction [21,45]. Myosin movements along actin filaments would also play a role in the stress fiber assembly [59]. However, these mechanisms do not provide the reason for the non-uniform MLC concentration and activation. Interestingly, structural mechanics-based considerations (Deguchi, unpublished data) indicate that a higher stretching strain is produced in central than in peripheral regions because a certain frictional force should be present at the interface between a stress fiber and surrounding cytoplasm when there is a relative displacement to each other [9,35,47]. Such non-uniform deformations can appear even without the assumptions on

non-uniform signal concentrations or non-uniform contractile/mechanical properties depending on the positions in the stress fiber, as were postulated in previous reports [2,41,55]. Thus, tension in stress fibers may not be distributed uniformly along the axial length. This theoretical consideration could also explain the mechanism of the spatially non-uniform molecular exchange activities of myosin and α-actinin in non-motile cells where molecular exchanges are more frequent in central regions [49], because a high (but physiological) stretching strain seems to induce frequent molecular turnovers [16,63,64].

6. Biomechanical properties characterized *in vitro*

Though stress fibers are highly dynamic in the cytoplasm as mentioned earlier, Katoh et al. [29] demonstrated that stress fibers isolated from fibroblasts, by low ionic strength solution and detergent extractions, are stable and are not disassembled even without tension. The use of isolated stress fibers thus helps understand the component composition and characterization of the mechanical properties excluding effects of the surrounding cytoplasm and turnovers. The isolated stress fiber showed contractile behavior whose magnitude was dependent on the concentration of Mg^{2+}-ATP. Detergent extraction using Triton X-100 readily dissolved both RhoA and Rho-kinase; hence, as mentioned earlier, such stress fibers showed only Ca^{2+}-dependent contractions. Meanwhile, fibers subjected to detergent extraction using glycerol were capable of contracting both in the presence and absence of Ca^{2+} since the Rho-kinase-mediated contraction, independent of Ca^{2+}, remained unchanged.

Surprisingly, the isolated stress fiber shortened to 20% of the original length, without molecular turnover or exchanges with cytoplasmic constituents [28,29]. Sarcomeres in striated muscles cannot shorten to that extent because of the existence of A-bands consisting mostly of myosin thick filaments (Fig. 4). Stress fibers in non-motile cells have a sarcomeric structure (Figs 2 and 3); yet, they may be less organized compared to the muscle sarcomere [12]. As for the difference between the stress fibers in non-motile cells and in muscle sarcomere, Peterson et al. [49] have proposed that α-actinin in stress fibers is not confined to a relatively narrow Z-line structure, but extends into an equivalent of the muscle I-band while binding to actin regions that do not overlap with myosin (Fig. 2).

In addition to the tension caused by isometric contraction, stress fibers in vascular endothelial and smooth muscle cells are subjected to cyclic stretching *in vivo* due to pulsatile blood pressure. Tensile properties of stress fibers are thus important to assess the resistance to the stretching and the ability of tension transmission that may directly activate remote mechanosensitive sites [17,22,43,60]. Using a pair of cantilevers as a micromanipulation tool, Deguchi et al. [8–10] evaluated a longitudinal elastic modulus of single stress fibers isolated from endothelial cells ($\sim$300 kPa) and smooth muscle cells ($\sim$1.45 MPa) assuming that stress fibers are a uniform structure having a certain cross-sectional area ($\sim$0.05 μm^2) estimated based on electron microscopy (Fig. 5). These values, even in the absence of Mg^{2+}-ATP that unties myosin from actin filaments, are much smaller in magnitude compared to single actin filaments having a longitudinal elastic modulus of $\sim$1 GPa [33]. Tensional loadings of $\sim$10-nN order of magnitude were required for stretching single stress fibers, whereas $\sim$100-pN tensions were enough for individual actin filaments to obtain their force–strain curves [37]. Since the slope of the force–strain curve (corresponding to elastic modulus) in Deguchi's data increases as stretch proceeds, stress fibers may have a loose structure in which dominant stress-bearing components vary with strain. Lu et al. [40] also reported a transverse elastic modulus of stress fibers in living cells that nonlinearly increased depending on the magnitude of substrate stretch.

The single proteins (i.e., actin filaments) and composite structures (i.e., stress fibers) thus differ in elastic modulus and force transmission ability. Cramer et al. [7] found that stress fibers in motile cells

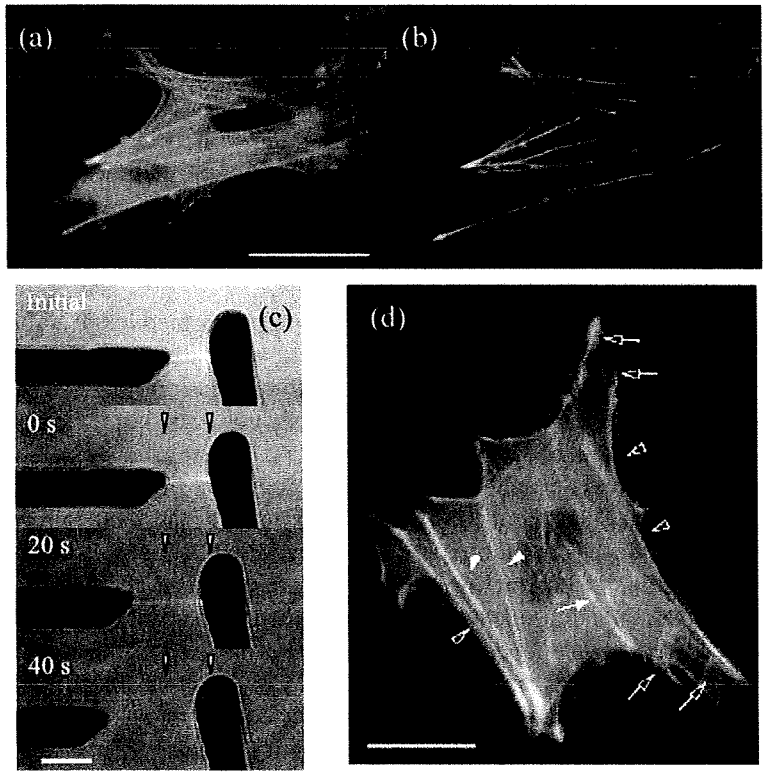

Fig. 5. Measurements on isolated stress fibers. (a) A smooth muscle cells expressing GFP-actin and RFP-focal adhesion kinase. (b) The same cell after cytoplasmic constituents are removed by chemical treatments except for the remaining stress fibers and focal adhesions. (c) Tensile test of a single stress fiber. Arrows indicate the initial positions of the cantilevers used for micromanipulation. (d) Superimposed images of smooth muscle cells before (green) and after (red) the cytoplasm except for ventral stress fibers and focal adhesions that were removed by chemical treatments. Some stress fibers (open arrowheads) were removed after the treatment, and thick stress fibers (closed arrowheads) pivoted outward. The positions of focal adhesions located at the terminal of stress fibers remained unchanged as shown by the yellow color. This result indicates that before the removal of the cytoplasm stress fibers had tensional prestress, and that they deform to reduce strain energy after some constraints are removed. Scale bars: 20 μm. Reproduced with permission of the copyright holder (Tech Science Press). (The colors are visible in the online version of the article.)

contain ~10–30 actin filaments. However, as far as the authors know, quantification of the number of associated filaments inside stress fibers of non-motile cells has not yet been achieved, although the amounts of respective molecular compositions within stress fibers were investigated [29]. As detailed mechanical structure (including boundary conditions between structural molecules) and force transmission inside stress fibers are largely unknown [1], qualitative and quantitative understating of such mechanical hierarchies will be a subject of future investigations.

7. Concluding remarks

In this review, starting from the clarification of which actin bundles are the subject of interest here, we discussed the biomechanical properties of stress fibers of non-motile cells, including isometric contraction, prestrain/prestress, elastic properties, and the relationships between those properties and the

dynamic exchanges of associated molecules occurring frequently in the cytoplasm. By keeping an intracellular mechanical homeostasis through the maintenance of the isometric contraction or remodeling of focal adhesions and stress fibers, cells seem to adapt to the surrounding mechanical environment.

Acknowledgements

The authors thank Kazushi Ito and Tsubasa Matsui for discussions. The authors apologize to workers in this field for having omitted many important papers owing to space constraints.

References

[1] M. Bathe, C. Heussinger, M.M.A.E. Claessens, A.R. Bausch et al., Cytoskeletal bundle mechanics, *Biophys. J.* **94** (2008), 2955–2964.
[2] A. Besser and U. Schwarz, Coupling biochemistry and mechanics in cell adhesion: a model for inhomogeneous stress fiber contraction, *New J. Phys.* **9** (2007), 1–27.
[3] K. Burridge, M. Chrzanowska-Wodnicka and C. Zhong, Focal adhesion assembly, *Trends Cell. Biol.* **7** (1997), 342–347.
[4] P.J. Cavnar, S.G. Olenych and T.C. Keller, Molecular identification and localization of cellular titin, a novel titin isoform in the fibroblast stress fiber, *Cell Motil. Cytoskel.* **64** (2007), 418–433.
[5] P. Chardin, P. Boquet, P. Madaule, M.R. Popoff et al., The mammalian G protein rhoC is ADP-ribosylated by clostridium botulinum exoenzyme C3 and affects actin microfilaments in vero cells, *EMBO J.* **8** (1989), 1087–1092.
[6] K.D. Costa, W.J. Hucker and F.C. Yin, Buckling of actin stress fibers: a new wrinkle in the cytoskeletal tapestry, *Cell Motil. Cytoskel.* **52** (2002), 266–274.
[7] L.P. Cramer, M. Siebert and T.J. Mitchison, Identification of novel graded polarity actin filament bundles in locomoting heart fibroblasts: implications for the generation of motile force, *J. Cell Biol.* **136** (1997), 1287–1305.
[8] S. Deguchi, T. Ohashi and M. Sato, Evaluation of tension in actin bundle of endothelial cells based on preexisting strain and tensile properties measurements, *Mol. Cell. Biomech.* **2** (2005), 125–133.
[9] S. Deguchi, T. Ohashi and M. Sato, Intracellular stress transmission through actin stress fiber network in adherent vascular cells, *Mol. Cell. Biomech.* **2** (2005), 205–216.
[10] S. Deguchi, T. Ohashi and M. Sato, Tensile properties of single stress fibers isolated from cultured vascular smooth muscle cells, *J. Biomech.* **39** (2006), 2603–2610.
[11] A.A. Dlugosz, P.B. Antin, V.T. Nachimas and H. Holtzer, The relationship between stress-fibre-like structures and nascent myofibrils in cultured cardiac myocytes, *J. Cell Biol.* **99** (1984), 2268–2278.
[12] Y.C. Fung, *Biomechanics Motion, Flow, Stress, and Growth*, Springer-Verlag, 1990, pp. 158–159.
[13] C.G. Galbraith and M.P. Sheetz, Forces on adhesive contacts affect cell function, *Curr. Opin. Cell Biol.* **10** (1998), 566–571.
[14] C.G. Galbraith and M.P. Sheetz, Keratocytes pull with similar forces on their dorsal and ventral surfaces, *J. Cell Biol.* **147** (1999), 1313–1324.
[15] B. Geiger and A. Bershadsky, Assembly and mechanosensory function of focal contacts, *Curr. Opin. Cell Biol.* **13** (2001), 584–592.
[16] J.M. Goffin, P. Pittet, G. Csucs, J.W. Lussi et al., Focal adhesion size controls tension-dependent recruitment of alpha-smooth muscle actin to stress fibers, *J. Cell Biol.* **172** (2006), 259–268.
[17] K. Hayakawa, H. Tatsumi and M. Sokabe, Actin stress fibers transmit and focus force to activate mechanosensitive channels, *J. Cell Sci.* **121** (2008), 496–503.
[18] B. Hinz, G. Celetta, J.J. Tomasek, G. Gabbiani and C. Chaponnier, Alpha-smooth muscle actin expressions upregulates fibroblast contractile activity, *Mol. Biol. Cell* **12** (2001), 2730–2741.
[19] B. Hinz and G. Gabbiani, Mechanisms of force generation and transmission by myofibroblasts, *Curr. Opin. Biotechnol.* **14** (2003), 538–546.
[20] H. Hirata, H. Tatsumi and M. Sokabe, Dynamics of actin filaments during tension-dependent formation of actin bundles, *Biochim. Biophys. Acta* **1770** (2007), 1115–1127.
[21] P. Hotulainen and P. Lappalainen, Stress fibers are generated by two distinct actin assembly mechanisms in motile cells, *J. Cell Biol.* **173** (2006), 383–394.
[22] S. Hu, J. Chen, B. Fabry, Y. Numaguchi et al., Intracellular tomography reveals stress focusing and structural anisotropy in cytoskeleton of living cells, *Am. J. Physiol. Cell Physiol.* **285** (2003), C1082–C1090.

[23] J.D. Humphrey, Vascular adaptation and mechanical homeostasis at tissue, cellular, and sub-cellular levels, *Cell Biochem. Biophys.* **50** (2008), 53–78.
[24] N. Inagaki, M. Nishizawa, M. Ito, M. Fujioka et al., Myosin binding subunit of smooth muscle myosin phosphatase at the cell–cell adhesion sites in MDCK cells, *Biochem. Biophys. Res. Commun.* **230** (1997), 552–556.
[25] D.E. Ingber, Tensegrity II. How structural networks influence cellular information processing networks, *J. Cell Sci.* **116** (2003), 1397–1408.
[26] Y. Kano, K. Katoh and K. Fujiwara, Lateral zone of cell–cell adhesion as the major fluid shear stress-related signal transduction site, *Circ. Res.* **86** (2000), 425–433.
[27] Y. Kano, K. Katoh, M. Masuda and K. Fujiwara, Macromolecular composition of stress fiber-plasma membrane attachment sites in endothelial cells *in situ*, *Circ. Res.* **79** (1996), 1000–1006.
[28] K. Katoh, Y. Kano, M. Amano, H. Onishi et al., Rho-kinase-mediated contraction of isolated stress fibers, *J. Cell Biol.* **153** (2001), 569–583.
[29] K. Katoh, Y. Kano, M. Masuda, H. Onishi and K. Fujiwara, Isolation and contraction of the stress fiber, *Mol. Biol. Cell* **9** (1998), 1919–1938.
[30] K. Katoh, M. Masuda, Y. Kano, Y. Jinguji and K. Fujiwara, Focal adhesion proteins associated with apical stress fibers of human fibroblasts, *Cell Motil. Cytoskel.* **31** (1995), 177–195.
[31] R. Kaunas, P. Nguyen, S. Usami and S. Chien, Cooperative effects of Rho and mechanical stretch on stress fiber organization, *Proc. Natl. Acad. Sci. USA* **102** (2005), 15895–15900.
[32] A. Kishino and T. Yanagida, Force measurements by micromanipulation of a single actin filament by glass needles, *Nature* **334** (1988), 74–76.
[33] H. Kojima, A. Ishijima and T. Yanagida, Direct measurement of stiffness of single actin filaments with and without tropomyosin by *in vitro* nanomanipulation, *Proc. Natl. Acad. Sci. USA* **91** (1994), 12962–12966.
[34] Y.E. Kreis and W. Birchmeier, Stress fiber sarcomeres of fibroblasts are contractile, *Cell* **22** (1980), 555–561.
[35] S. Kumar, I.Z. Maxwell, A. Heisterkamp, T.R. Polte et al., Viscoelastic retraction of single living stress fibers and its impact on cell shape, cytoskeletal organization, and extracellular matrix mechanics, *Biophys. J.* **90** (2006), 3762–3773.
[36] E. Lazarides and K. Burridge, α-Actinin: immunofluorescent localization of a muscle structural protein in nonmuscle cells, *Cell* **6** (1975), 289–298.
[37] X. Liu and G.H. Pollack, Mechanics of F-actin characterized with microfabricated cantilevers, *Biophys. J.* **83** (2002), 2705–2715.
[38] C.M. Lloyd, M.M. Berendse, D.G. Lloyd, G. Schevzov and M.D. Grounds, A novel role for non-muscle γ-actin in skeletal muscle sarcomere assembly, *Exp. Cell Res.* **297** (2002), 82–96.
[39] L. Lu, Y. Feng, W.J. Hucker, S.J. Oswald, G.D. Longmore and F.C. Yin, Actin stress fiber pre-extension in human aortic endothelial cells, *Cell. Motil. Cytoskel.* **65** (2008), 281–294.
[40] L. Lu, S.J. Oswald, H. Ngu and F.C. Yin, Mechanical properties of actin stress fibers in living cells, *Biophys. J.* **95** (2008), 6060–6071.
[41] Y. Luo, X. Xua, T. Lele, S. Kumar and D.E. Ingber, A multi-modular tensegrity model of an actin stress fiber, *J. Biomech.* **41** (2008), 2379–2387.
[42] K. Murata, K. Hirano, E. Villa-Moruzzi, D.J. Hartshorne and D.L. Brautigan, Differential localization of myosin and myosin phosphatase subunits in smooth muscle cells and migrating fibroblasts, *Mol. Biol. Cell* **8** (1997), 663–673.
[43] S. Na, O. Collin, F. Chowdhury, B. Tay et al., Rapid signal transduction in living cells is a unique feature of mechanotransduction, *Proc. Natl. Acad. Sci. USA* **105** (2008), 6626–6631.
[44] S. Na, G.A. Meininger and J.D. Humphrey, Theoretical model for F-actin remodeling in vascular smooth muscle cells subjected to cyclic stretch, *J. Theor. Biol.* **246** (2007), 87–99.
[45] P. Naumanen, P. Lappalainen and P. Hotulainen, Mechanisms of actin stress fibre assembly, *J. Microsc.* **231** (2008), 446–454.
[46] K. Ohashi, K. Nagata, M. Maekawa, T. Ishizaki et al., Rho-associated kinase ROCK activates LIM-kinase 1 by phosphorylation at threonine 508 within the activation loop, *J. Biol. Chem.* **275** (2000), 3577–3582.
[47] E.A. Osborn, A. Rabodzey, C.F. Dewey Jr. and J.H. Hartwig, Endothelial actin cytoskeleton remodeling during mechanostimulation with fluid shear stress, *Am. J. Physiol. Cell Physiol.* **290** (2006), C444–C452.
[48] S. Pellegrin and H. Mellor, Actin stress fibres, *J. Cell Sci.* **120** (2007), 3491–3499.
[49] L.J. Peterson, Z. Rajfur, A.S. Maddox, C.D. Freel et al., Simultaneous stretching and contraction of stress fibers *in vivo*, *Mol. Biol. Cell* **15** (2004), 3497–3508.
[50] A.J. Ridley and A. Hall, The small GTP-binding protein rho regulates the assembly of focal adhesions and actin stress fibers in response to growth factors, *Cell* **70** (1992), 389–399.
[51] J.W. Sanger, J.M. Sanger and B.M. Jockusch, Differences in the stress fibers fibroblasts and epithelial cells, *J. Cell Biol.* **96** (1983), 961–969.
[52] K. Sato, T. Adachi, M. Matsuo and Y. Tomita, Quantitative evaluation of threshold fiber strain that induces reorganization of cytoskeletal actin fiber structure in osteoblastic cells, *J. Biomech.* **38** (2005), 1895–1901.

[53] T. Shemesh, B. Geiger, A.D. Bershadsky and M.M. Kozlov, Focal adhesions as mechanosensors: a physical mechanism, *Proc. Natl. Acad. Sci. USA* **102** (2005), 12383–12388.
[54] M. Sokabe, K. Hayakawa and H. Tatsumi, Differentiation of two types of mechanosensors in endothelial cells, *J. Biomech.* **39** (2006), S311.
[55] M.R. Stachowiak and B. O'Shaughnessy, Kinetics of stress fibers, *New J. Phys.* **10** (2008), 025002.
[56] A.F. Straight, A. Cheung, J. Limouze, I. Chen et al., Dissecting temporal and spatial control of cytokinesis with a myosin II inhibitor, *Science* **299** (2003), 1743–1747.
[57] J.L. Tan, J. Tien, D.M. Pirone, D.S. Gray et al., Cells lying on a bed of microneedles: an approach to isolate mechanical force, *Proc. Natl. Acad. Sci. USA* **100** (2003), 1484–1489.
[58] Y. Tsuda, H. Yasutake, A. Ishijima and T. Yanagida, Torsional rigidity of single actin filaments and actin–actin bond breaking force under torsion measured directly by *in vitro* micromanipulation, *Proc. Natl. Acad. Sci. USA* **93** (1996), 12937–12942.
[59] A.B. Verkhovsky, T.M. Svitkina and G.G. Borisy, Polarity sorting of actin filaments in cytochalasin-treated fibroblasts, *J. Cell Sci.* **110** (1997), 1693–1704.
[60] N. Wang and Z. Suo, Long-distance propagation of forces in a cell, *Biochem. Biophys. Res. Commun.* **328** (2005), 1133–1138.
[61] T. Watanabe, H. Hosoya and S. Yonemura, Regulation of myosin II dynamics by phosphorylation and dephosphorylation of its light chain in epithelial cells, *Mol. Biol. Cell* **18** (2007), 605–616.
[62] B. Wojciak-Stothard and A.J. Ridley, Shear stress-induced endothelial cell polarization is mediated by Rho and Rac but not Cdc42 or PI 3-kinases, *J. Cell Biol.* **161** (2003), 429–439.
[63] M. Yoshigi, L.M. Hoffman, C.C. Jensen, H.J. Yost and M.C. Beckerle, Mechanical force mobilizes zyxin from focal adhesions to actin filaments and regulates cytoskeletal reinforcement, *J. Cell Biol.* **171** (2005), 209–215.
[64] C. Zhong, M. Chrzanowska-Wodnicka, J. Brown, A. Shaub et al., Rho-mediated contractility exposes a cryptic site in fibronectin and induces fibronectin matrix assembly, *J. Cell Biol.* **141** (1998), 539–551.

Biochemical and Biophysical Research Communications 394 (2010) 94–99

Contents lists available at ScienceDirect

Biochemical and Biophysical Research Communications

journal homepage: www.elsevier.com/locate/ybbrc

Direct measurement of shear strain in adherent vascular endothelial cells exposed to fluid shear stress

Yosuke Ueki [a,b,*], Naoya Sakamoto [a], Masaaki Sato [a,c]

[a] Department of Bioengineering and Robotics, Graduate School of Engineering, Tohoku University, Japan
[b] Research Fellow of the Japan Society for the Promotion of Science, Japan
[c] Department of Biomedical Engineering, Graduate School of Biomedical Engineering, Tohoku University, Japan

ARTICLE INFO

Article history:
Received 17 February 2010
Available online 20 February 2010

Keywords:
Endothelial cell
Fluid shear stress
Shear modulus
Force transmission
Confocal microscopy

ABSTRACT

Functional and morphological responses of endothelial cells (ECs) to fluid shear stress are thought to be mediated by several mechanosensitive molecules. However, how the force due to fluid shear stress applied to the apical surface of ECs is transmitted to the mechanosensors is poorly understood. In the present paper, we performed an analysis of an intracellular mechanical field by observation of the deformation behaviors of living ECs exposed to shear stress with a novel experimental method. Lateral images of human umbilical vein ECs before and after the onset of flow were obtained by confocal microscopy, and image correlation and finite element analysis were performed for quantitative analyses of subcellular strain due to shear stress. The shear strain of the cells changed from 1.06 ± 1.09% (mean ± SD) to 4.67 ± 1.79% as the magnitude of the shear stress increased from 2 to 10 Pa. The nuclei of ECs also exhibited shear deformation, which was similar to that observed in cytoplasm, suggesting that nuclei transmit forces from apical to intracellular components, as well as cytoskeletons. The obtained strain–stress relation resulted in a mean shear modulus of 213 Pa for adherent ECs. These results provide a mechanical perspective on the investigation of flow-sensing mechanisms of ECs.

© 2010 Elsevier Inc. All rights reserved.

1. Introduction

Hemodynamic fluid shear stress (FSS) acting on vascular endothelial cells (ECs) evokes a variety of cellular responses, including proliferation [1], expression of adhesive molecules [2], cytoskeletal structures and morphology [3], and mechanical properties [4] that may be relevant to both the physiology and pathology of blood vessels. Thus, numerous previous studies have attempted to determine the mechanism by which ECs sense FSS and adapt to mechanical environments. Recently, FSS-induced activation of several of the candidate mechanosensitive molecules, such as G proteins [5] and PECAM-1 [6], has been demonstrated. However, as of yet, there is no primary evidence as to whether these molecules are activated directly by mechanical loading or by intracellular signaling interactions that were cued by another mechanosensor. This is thought to be due to the difficulties in precisely describing the intracellular mechanical conditions, i.e., how FSS acting on the apical surface of ECs is transmitted and generates an intracellular mechanical field. As such, it is necessary to investigate the degree to which forces are exerted on the intercellular junction, focal adhesions, and other candidates for mechanotransducers.

Helmke et al. [7,8] reported the flow-induced displacement of intermediate filaments downstream of the flow and calculated the intracellular strain field from movements of cytoskeletal networks. However, they could not clearly distinguish the passive deformation of cells from the active response of cells via biochemical responses. This may be one of the difficulties in experimentally revealing the mechanism of FSS-sensing by ECs. Numerical approaches are efficient methods by which to overcome the difficulty of separating passive deformation from active cell movements. Some previous reports have used computational analysis to evaluate the mechanical environment of ECs exposed to FSS [9,10]. Ferko et al. [10] reported a method for analyzing the intracellular strain fields of ECs exposed to shear flow using a cell-specific finite element model, in which the subcellular structures of the nucleus and focal adhesions were incorporated. However, these computational studies could not reveal the actual intracellular mechanical environment at the subcellular level because living cells have more complicated internal structures, such as cytoskeletons, which may contribute to intercellular force transmission and mechanical properties [11,12]. In addition, the actual shear modulus of cells, which is a critical determinant of the shear-induced deformation of cells, is thought to be different from the theoretical value

* Corresponding author. Address: Department of Bioengineering and Robotics, Graduate School of Engineering, Tohoku University, 6-6-01, Aramaki-aoba, Aoba-ward, Sendai City, Japan. Fax: +81 22 795 6945.
E-mail address: ueki@biml.mech.tohoku.ac.jp (Y. Ueki).

0006-291X/$ - see front matter © 2010 Elsevier Inc. All rights reserved.
doi:10.1016/j.bbrc.2010.02.115

computed from Young's modulus with the assumptions of isotropy and incompressibility, while the modulus has been used in almost all computational studies.

In an attempt to solve this problem, in the present study, we report a novel experimental technique that enables direct observation of the passive deformation of living ECs exposed to the physiological range of FSS by confocal microscopy and the measurement of the intracellular strain field together with the application of image processing and the finite element method (FEM). To reveal the role of actin filaments in force bearing in ECs exposed to FSS, the deformation behavior of ECs treated with cytochalasin D is also analyzed. In addition, we calculate the shear modulus of ECs and measure the shear strain of ECs exposed to FSS controlled to physiological magnitudes.

2. Materials and methods

2.1. Cell culture and fluorescent labeling

Human umbilical vein endothelial cells (HUVECs) isolated from umbilical veins by trypsin treatment, as described in a previous study [13], were grown in Medium 199 (Invitrogen) containing 20% fetal bovine serum (JRH Biosciences), 10 ng/ml basic fibroblast growth factor (Austral Biologicals), and penicillin–streptomycin (Invitrogen). For the experiment, cells were seeded on a ϕ35-mm glass-bottom dish (with a ϕ12-mm hole on the bottom and covered with a ϕ27-mm cover glass, AGC Techno Glass) pre-coated with 0.1% bovine gelatin (Sigma–Aldrich). The following experiments were conducted after the cells achieved confluence.

Two hours before the experiment, the cytoplasmic domain and nuclei of living HUVECs were stained with 10 μM Cell Tracker Red CMTPX (Invitrogen) and 5 μM SYTO13 (Invitrogen), respectively. These fluorescent dyes induced speckled patterns of labeling, which are suitable for the image correlation described later herein.

In order to evaluate the role of actin cytoskeletons in FSS-induced deformations, HUVECs were treated with 0.2 or 2 μM cytochalasin D (CytoD, Enzo Life Sciences), which is a commonly used regent for the inhibition of actin polymerization, for 30 min prior to the experiments.

2.2. Experimental setup and procedure

The flow-exposure system consisting of a parallel plate flow chamber, a syringe pump (KDS210, KD Scientific), a tube heater (MATS-TH, Tokai hit), and polyethylene tubes (Imamura) was used in the present study (Fig. 1). The flow chamber was composed of a cell culture dish, a polycarbonate I/O unit, and a silicone gasket, which determines the geometry of the flow section of 0.2 mm in height and 2 mm in width. The mean shear stress acting on the HUVEC monolayer is expressed as

$$\tau = 6\mu Q/bh^2, \quad (1)$$

where μ is the viscosity of the culture medium, which was 0.74 mPa s (at 37 °C) as measured with a sine wave vibro-viscometer (SV10, A&D), Q is the flow rate, and h and b are the flow channel height and width, respectively. The flow rate driven by the pump was controlled to expose the HUVEC monolayer to FSS of desired magnitudes. To maintain the appropriate pH during the experiments in a low CO_2 atmosphere (room atmosphere), the medium was replaced into M199 with Hanks' salts (Invitrogen). For the CytoD-treated experiment, the same concentration of CytoD used to pre-treat the HUVECs was added to the medium. The chamber was mounted on a stage equipped with a thermo-control system (MI-IBC, Olympus) of an inverted confocal laser scanning microscope (CLSM, FV1000, Olympus). The temperature of the medium was maintained at between 35 and 37 °C by means of the tube heater and the thermo-control system. Lateral images of HUVECs were obtained using a 100× objective lens (UplanApo, NA = 1.35, Olympus) in line scanning mode at a pixel resolution of 124 nm/pixel and a vertical spacing of 120 nm/pixel. Based on the Rayleigh criterion, the optical horizontal resolution was 226 nm at a wavelength of 500 nm. The image size was approximately 1000 pixels (horizontal) × 150 pixels (vertical), and the time required for scanning was 3–4 s/frame. The scanning line was set to be parallel to the direction of flow crossing the vicinity of the center of the nucleus and containing two to four HUVECs in one frame. A personal computer (NJ2150, Epson Direct) with a custom Labview 8.6 (National Instruments) program was used to synchronize the pushing motion of the syringe pump and the trigger signal for image acquisition by CLSM for a temporally well-coordinated measurement.

Fig. 1B shows the experimental regime for measurements of cell deformation. Based on the intracellular stress tomography reported by Hu et al. [11], we used intermittent patterns of FSS exposure and image acquisition, which was phase-locked to the periodic FSS exposure, for precise measurement of the intracellular mechanical field. The square-wave form pattern of FSS with a frequency of 0.05 Hz, which corresponds to the alternating repetition of a 10 s FSS exposure and a 10 s pause of FSS, were applied to ECs. Trigger signals for image acquisition were input to the CLSM at 5 s after onset and offset of flow. This 20 s cycle of flow pattern and image acquisition was repeated five times at the same FSS level. Therefore, we obtained five "deformed" and five "undeformed" lateral images of HUVECs. This procedure facilitated the reduction of the effect of random movement of intracellular structures and active deformation of cells due to cell migration. This five-cycle repetition was performed sequentially while varying the maximum FSS as 2, 4, 6, and 10 Pa, so that the deformation of identical cells could be measured under various shear stress levels.

2.3. Image correlation

To obtain the intracellular displacement field, an image correlation analysis was carried out between the undeformed and deformed images. Prior to the analysis, the following image processing was performed using ImageJ 1.40b software (National Institutes of Health). First, the parallel displacement in the vertical direction of the cells in the lateral images were corrected because the change in internal pressure of the chamber due to flow induced the deflection of the glass bottom, resulting in a vertical shift of the images. The center-of-mass of the cross section of the cells was detected with the "Analyze particle" function of ImageJ. Based on these obtained drift data, the vertical positions of the images were corrected using the "Translate" function of ImageJ with sub-pixel interpolation. Then, the aspect ratio of the images was corrected from 0.124:0.120 (horizontal:vertical) to 1:1. Finally, the averaged images were generated from "deformed" and "undeformed" images, respectively, using the image calculation function of ImageJ in order to reduce the noise.

Displacement vectors of each pixel in lateral images were obtained from a pair of averaged "deformed" and "undeformed" images with an image correlation method using Flow-vec 2.8 software (Library). A small region of 13 × 13 pixels surrounding the object pixel was set as the sample window. The displacement of each window was detected with a spatial resolution of approximately 1/10 pixel, corresponding to approximately 12 nm.

2.4. FEM analysis

FEM analysis was performed to calculate the strain field from the displacement field using ANSYS 11.0 multipurpose FEM analysis software (ANSYS). Conversion of image data to the finite element model was performed as follows. All pixels in an image

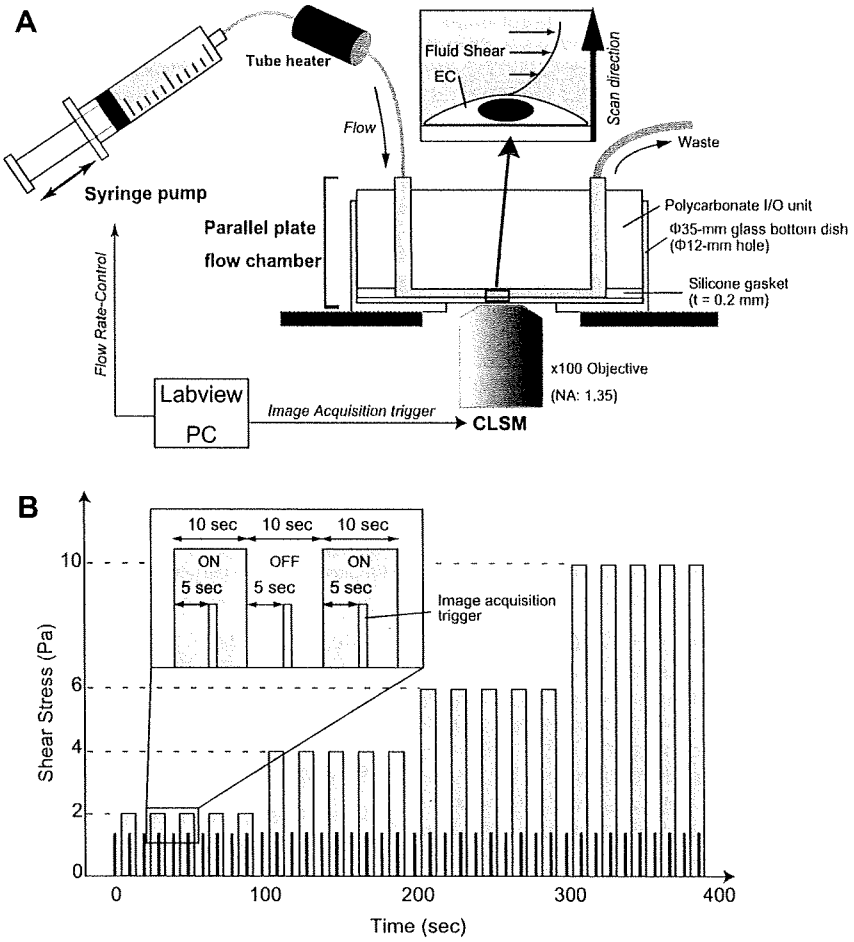

Fig. 1. Experimental setup and procedure. (A) Schematic diagram of the experimental setup for visualization of FSS-induced deformation of ECs. A parallel plate flow chamber is illustrated in a cross-sectional view. (B) Diagram of the experimental regime. A HUVEC monolayer was exposed to square-wave form FSS with a frequency of 0.05 Hz, a duty cycle of 50%, and amplitudes of 2, 4, 6, and 10 Pa.

were converted into nodes of four-node shell elements in FEM, and the vectors obtained from image correlation were allocated to nodes as constraint displacements. After the obtaining the solution, we obtained the shear strain in each pixel as nodal solutions.

2.5. Calculation of shear modulus

To calculate the shear modulus of adherent HUVECs, the mean shear strain of a cell was calculated by averaging the shear strains of all pixels on the cells. Therefore, the shear modulus (G) can be calculated using following simple equation, which is the definition of shear modulus:

$$\tau = G\gamma, \tag{2}$$

where τ is the applied FSS and γ is the mean shear strain.

3. Results and discussion

3.1. FSS-induced deformation of ECs

In the present study, we observed the deformation of ECs exposed to FSS by confocal microscopy. As shown in Movie S1 (in Supplementary material), we successively observed the deformation behavior of ECs under a shear stress of 2–10 Pa. Fig. 2 shows representative lateral views of fluorescent images of ECs (Fig. 2A–H), displacement fields (Fig. 2I–L), and shear strain fields (Fig. 2M–P). As shown in Fig. 2I–L (particularly clearly in Fig. 2K and L), large displacements (of up to 600 nm) were observed at the apical side of the cells, whereas the displacements of the bottom sides were small compared to the apical side. The difference in displacement between the apical and basal sides provides a direct indication of the shear deformation of cells. To our knowledge, this is the first report of the direct measurement of shear deformation of adherent ECs exposed to FSS. Helmke et al. [7,8] observed the FSS-induced deformation of ECs using an experimental procedure similar to that of the present study. They analyzed the total passive and active cell deformation that occurred 3 min after flow onset. On the other hand, in the present study, from the total deformation, we extracted only the displacements due to passive deformation that occurred 10 s after flow onset. Therefore, to our knowledge, the observation of the present study is the first to distinguish passive deformation from the active responses of ECs exposed to FSS.

As shown in Fig. 2A through, the greater part of the lateral images of the HUVECs was occupied by nuclei, and the shear deformation of the cell was accompanied by deformation of the nucleus (Fig. 2E–H, Movie S1). The shear strain mappings shown in Fig. 2M–P had scattered distributions, and no difference in the magnitude of shear strain between the cytoplasm and the nuclei was observed. According to previous reports [14,15], the nucleus is approximately 2.5–16 times stiffer than the cytoplasm. These results suggest the existence of mechanical connections between the

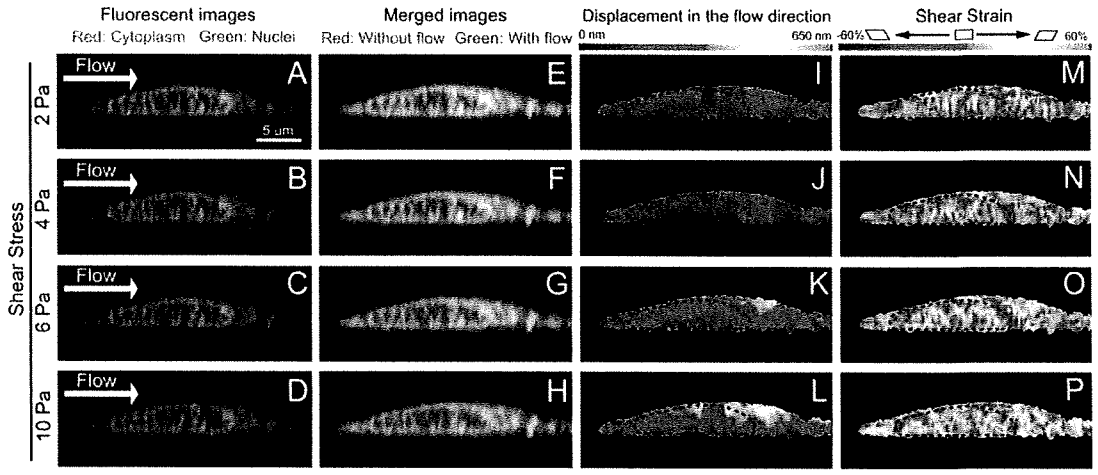

Fig. 2. Lateral images of HUVECs exposed to FSSs of 2 Pa (A, E, I, and M), 4 Pa (B, F, J, and N), 6 Pa (C, G, K, and O), and 10 Pa (D, H, L, and P). (A–D) Fluorescent images of nuclei (green) and cytoplasm (red) of HUVECs under given FSS. (E–H) Merged images of HUVECs under static (red) and flow (green) conditions. Disagreement of green and red colors indicates the displacement due to the flow. (I–L) Contour mappings of displacement in the flow direction. (M–P) Contour mappings of shear strain analyzed using FEM. The dextral and sinistral shear strains are indicated by warm and cold colors, respectively. (For interpretation of the references to color in this figure legend, the reader is referred to the web version of this paper.)

apical surface and the basal side via the nucleus transmitting forces. Crisp et al. [16] reported a structural linkage between the actin cytoskeleton and the nuclei via nesprin molecules, and Wang et al. [17] suggested that this connection contributes to the force transmission from the extracellular matrix to the nuclei. Taken together, the nucleus can act not only as a mechanosensor but also as a force transmitter as well as a cytoskeletal structure [11], which is known to transmit forces on the apical surface to focal adhesions containing several candidate mechanosensitive molecules.

3.2. Shear modulus of HUVECs

The mean shear strain level in each cell was increased proportional to the magnitude of FSS applied, as indicated in Fig. 3. The shear strain was 1.03 ± 1.09% (mean ± SD) at 2 Pa and increased to 4.67 ± 1.79% at 10 Pa. These values correspond to shear angles of 0.59° and 2.67°, respectively. From the linear relationship between the applied FSS (τ) and the shear strain (γ), we obtained following relationship:

$$\gamma\ [\%] = 1/G \cdot 100 \cdot \tau = 0.469 \cdot \tau\ [\text{Pa}]. \quad (3)$$

Then, the shear modulus (G) of HUVECs is expressed as follows:

$$G = 1/0.469 \cdot 100 = 213\ [\text{Pa}]. \quad (4)$$

We can also obtain the shear modulus of the cell from Young's modulus (E) from the following equation under the assumptions of incompressibility and isotropy, as follows:

$$G = E/2(1 + \nu), \quad (5)$$

where ν is Poisson's ratio. Under the assumption of incompressibility ($\nu = 0.5$), we obtain:

$$G = E/3. \quad (6)$$

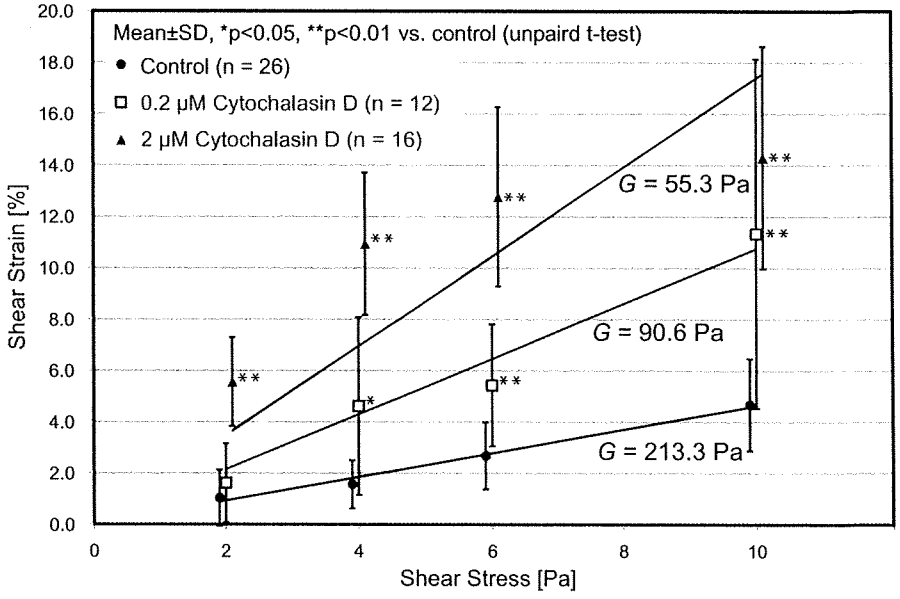

Fig. 3. Relationship between the applied FSS and the shear strain of HUVECs. Control cells (closed circles), 0.2 μM CytoD treated cells (open squares), and 2 μM CytoD treated cells (closed triangles).

Kataoka et al. [18] and Mathur et al. [14] measured the Young's modulus of HUVECs by indentation measurement using atomic force microscope (AFM) and reported the Young's modulus to be in the range of 3–6 kPa, which, based on Eq. (6), yields a shear modulus in the range of from 1 to 2 kPa. Therefore, the shear modulus obtained in the present study is considered to be smaller than the value calculated from the previously reported Young's modulus under the assumptions of incompressibility and isotropy. Although the reason for this difference is unclear, a number of possibilities have been suggested. First, the limitation of the assumption of isotropy has been suggested to induce the difference in the values. Hu et al. [19] reported that the anisotropic mechanical property of adherent cells depends on actin cytoskeletons. Second, we calculated the shear modulus under the assumption that the average shear stresses of 2, 4, 6, and 10 Pa induced shear strain in the ECs. However, it has been reported that shear stresses acting on the EC surface are nonuniformly distributed, depending on the surface topography of ECs, and that a maximum shear stress greater than mean is exerted at the apex of ECs [10,20]. In the present study, we averaged the shear strain in each pixel of a cell in calculating the mean shear strain in a cell. If FSS increases at the apex region of ECs, the mean shear strain may have been overestimated because the local strain beneath the apex region, which occupies a large part of the vertical section of the ECs, would be much larger than the other part of the ECs and would have a significant effect on the mean value. Furthermore, the heterogeneity of the cell is thought to be the reason for this difference. Previous studies reporting the Young's modulus of HUVECs have used AFM. The Young's modulus obtained by AFM may be affected by the local stiffness of the cell surface, which contains a stiff cortical layer consisting primarily of actin filaments. On the other hand, the shear modulus presented in the present study is calculated from the strain over the entire area of the HUVEC.

3.3. Role of actin filaments in FSS-induced deformation

Fig. 4G–L and M–R shows the displacement fields and shear strain fields, respectively, of HUVECs treated with CytoD. Both displacement and shear strain increased with the increase in CytoD concentration. The maximum displacement was more than 2 μm, and the maximal shear strain exceeded 50% (both indicated in gray in the contour images) in the HUVECs treated using 2 μM CytoD exposed to 10 Pa. As shown in Fig. 3, the shear strain caused by FSS of the ECs increased significantly upon CytoD treatment. The shear moduli of HUVECs treated with 0.2 and 2 μM CytoD were 90.6 and 55.3 Pa, respectively. Wakatsuki et al. [21] reported the relationship between the normal stiffness of cells measured by indentation testing and the concentration of treated CytoD. According to their report, the normal stiffness decreased to approximately 40% and 15% when cells were treated with 0.2 μM CytoD and 2 μM CytoD, respectively. In the present study, treatment with CytoD of the same concentrations reduced the shear moduli to 42% and 25%, respectively. This result suggests that actin cytoskeleton contributes to the shear force bearing as well as the normal force.

Some previous studies have reported polarized biochemical responses in ECs exposed to FSS [22,23]. For example, Zaidel-Bar et al. [22] reported that FSS induces phosphorylation of paxillin at the downstream edge and inactivation of small GTPase Rac1 at the upstream side of ECs. In addition, we previously suggested that the directional remodeling of ECs are mediated by activation of mechanosensors in the localized region of a cell [24]. Taken together, locally concentrated forces are considered to be exerted on mechanosensors to induce the localized activation of the signal transduction leading to the directional remodeling of cells. Recent reports have suggested that the locally applied force transmitted through cytoskeletons induces rapid activation of Rac1 at the distal point from the point of application of the force [25], which suggests that force transmission via cytoskeletons may play an important role in the polarized activation of mechanosensors. However, in the present study, we did not investigate force transmission to an extracellular matrix or to adjacent cells. According to these findings and considerations, further investigations should include quantitative evaluations of force transmission to the candidates for mechanosensors, such as focal adhesions or intercellular junctions, and localized biological responses such as the activation of RhoGTPases [22,23,25] in order to demonstrate the correlation be-

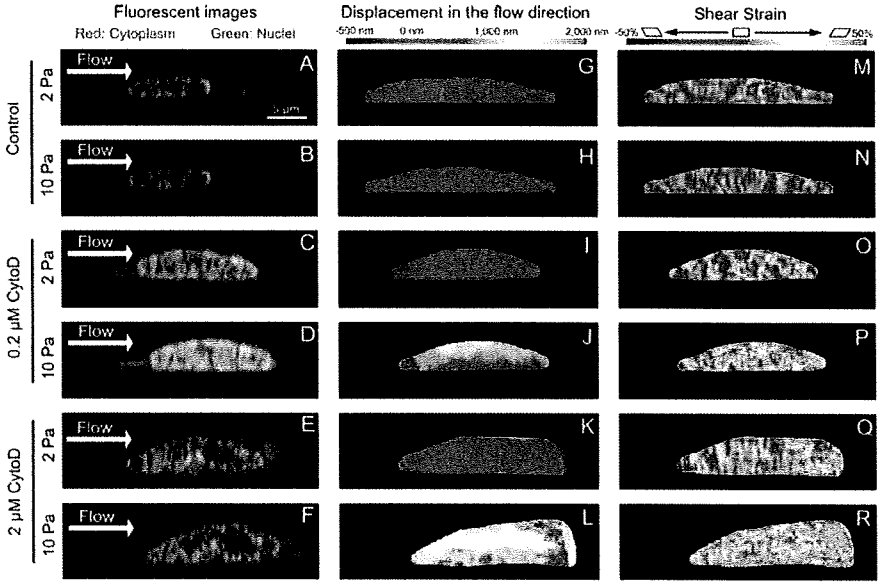

Fig. 4. Lateral images of HUVECs exposed to FSSs of 2 Pa (A, G, M, C, I, O, E, H, and Q) and 10 Pa (B, H, N, D, J, P, F, L, and R). (C, D, I, J, O, and P) HUVECs treated with 0.2 μM CytoD, and (E, F, K, L, Q, and R) HUVECs treated with 2 μM CytoD. (A–F) Fluorescent images of nucleus (green) and cytoplasm (red) of HUVECs under a given FSS. (G–L) Contour mapping of the displacement to the flow direction (left to right). (M–R) Contour mapping of the shear strain. The dextral and sinistral shear, strains are indicated by warm and cold colors, respectively. (For interpretation of the references to color in this figure legend, the reader is referred to the web version of this paper.)

tween mechanical fields and mechanotransduction in ECs exposed to FSS.

4. Conclusion

In the present study, we proposed a novel but simple technique to observe the passive shear deformation of living ECs exposed to FSS of physiological levels. Using image correlation and FEM analysis, we analyzed the subcellular strain field of ECs quantitatively and calculated the shear modulus of adherent ECs without any contacting probes. As a result, ECs and their nuclei were demonstrated to exhibit shear strain proportional to the applied FSS and the shear modulus of ECs was found to be 213 Pa.

Acknowledgments

The authors thank Dr. Ikuo Takahashi for kindly providing the human umbilical cords with the informed consent of donors. The present study was supported in part by Grants-in-Aid for Scientific Research from the Ministry of Education, Culture, Sports, Science and Technology (MEXT) of Japan (Nos. 20001007 and 21-3835).

Appendix A. Supplementary data

Supplementary data associated with this article can be found, in the online version, at doi:10.1016/j.bbrc.2010.02.115.

References

[1] M.J. Levesque, R.M. Nerem, E.A. Sprague, Vascular endothelial cell proliferation in culture and the influence of flow, Biomaterials 11 (1990) 702–707.
[2] M. Morigi, C. Zoja, M. Figliuzzi, M. Foppolo, G. Micheletti, M. Bontempelli, M. Saronni, G. Remuzzi, A. Remuzzi, Fluid shear stress modulates surface expression of adhesion molecules by endothelial cells, Blood 85 (1995) 1696–1703.
[3] C.G. Galbraith, R. Skalak, S. Chien, Shear stress induces spatial reorganization of the endothelial cell cytoskeleton, Cell Motil. Cytoskeleton 40 (1998) 317–330.
[4] M. Sato, K. Nagayama, N. Kataoka, M. Sasaki, K. Hane, Local mechanical properties measured by atomic force microscopy for cultured bovine endothelial cells exposed to shear stress, J. Biomech. 33 (2000) 127–135.
[5] S.R. Gudi, C.B. Clark, J.A. Frangos, Fluid flow rapidly activates G proteins in human endothelial cells. Involvement of G proteins in mechanochemical signal transduction, Circ. Res. 79 (1996) 834–839.
[6] E. Tzima, M. Irani-Tehrani, W.B. Kiosses, E. Dejana, D.A. Schultz, B. Engelhardt, G. Cao, H. DeLisser, M.A. Schwartz, A mechanosensory complex that mediates the endothelial cell response to fluid shear stress, Nature 437 (2005) 426–431.
[7] B.P. Helmke, D.B. Thakker, R.D. Goldman, P.F. Davies, Spatiotemporal analysis of flow-induced intermediate filament displacement in living endothelial cells, Biophys. J. 80 (2001) 184–194.
[8] B.P. Helmke, A.B. Rosen, P.F. Davies, Mapping mechanical strain of an endogenous cytoskeletal network in living endothelial cells, Biophys. J. 84 (2003) 2691–2699.
[9] T. Ohashi, H. Sugawara, T. Matsumoto, M. Sato, Surface topography measurement and intracellular stress analysis of cultured endothelial cells exposed to fluid shear stress, JSME Int. J. C Mech. Syst. Mach. Elem. Manuf. 43 (2000) 780–786.
[10] M.C. Ferko, A. Bhatnagar, M.B. Garcia, P.J. Butler, Finite-element stress analysis of a multicomponent model of sheared and focally-adhered endothelial cells, Ann. Biomed. Eng. 35 (2007) 208–223.
[11] S. Hu, J. Chen, B. Fabry, Y. Numaguchi, A. Gouldstone, D.E. Ingber, J.J. Fredberg, J.P. Butler, N. Wang, Intracellular stress tomography reveals stress focusing and structural anisotropy in cytoskeleton of living cells, Am. J. Physiol. Cell Physiol. 285 (2003) C1082–C1090.
[12] M. Sato, K. Suzuki, Y. Ueki, T. Ohashi, Microelastic mapping of living endothelial cells exposed to shear stress in relation to three-dimensional distribution of actin filaments, Acta Biomater. 3 (2007) 311–319.
[13] N. Sakamoto, T. Ohashi, M. Sato, Effect of magnetic field on nitric oxide synthesis of cultured endothelial cells, Int. J. Appl. Electromagn. Mech. 14 (2001) 317–322.
[14] A.B. Mathur, G.A. Truskey, W.M. Reichert, Atomic force and total internal reflection fluorescence microscopy for the study of force transmission in endothelial cells, Biophys. J. 78 (2000) 1725–1735.
[15] N. Caille, O. Thoumine, Y. Tardy, J.-J. Meister, Contribution of the nucleus to the mechanical properties of endothelial cells, J. Biomech. 35 (2002) 177–187.
[16] M. Crisp, Q. Liu, K. Roux, J.B. Rattner, C. Shanahan, B. Burke, P.D. Stahl, D. Hodzic, Coupling of the nucleus and cytoplasm: role of the LINC complex, J. Cell Biol. 172 (2006) 41–53.
[17] N. Wang, J.D. Tytell, D.E. Ingber, Mechanotransduction at a distance: mechanically coupling the extracellular matrix with the nucleus, Nat. Rev. Mol. Cell Biol. 10 (2009) 75–82.
[18] N. Kataoka, K. Iwaki, K. Hashimoto, S. Mochizuki, Y. Ogasawara, M. Sato, K. Tsujioka, F. Kajiya, Measurements of endothelial cell-to-cell and cell-to-substrate gaps and micromechanical properties of endothelial cells during monocyte adhesion, Proc. Natl. Acad. Sci. USA 99 (2002) 15638–15643.
[19] S. Hu, L. Eberhard, J. Chen, J.C. Love, J.P. Butler, J.J. Fredberg, G.M. Whitesides, N. Wang, Mechanical anisotropy of adherent cells probed by a three-dimensional magnetic twisting device, Am. J. Physiol. Cell Physiol. 287 (2004) C1184–C1191.
[20] T. Yamaguchi, Y. Yamamoto, H. Liu, Computational mechanical model studies on the spontaneous emergent morphogenesis of the cultured endothelial cells, J. Biomech. 33 (2000) 115–126.
[21] T. Wakatsuki, B. Schwab, N.C. Thompson, E.L. Elson, Effects of cytochalasin D and latrunculin B on mechanical properties of cells, J. Cell Sci. 114 (2001) 1025–1036.
[22] R. Zaidel-Bar, Z. Kam, B. Geiger, Polarized downregulation of the paxillin-p130CAS-Rac1 pathway induced by shear flow, J. Cell Sci. 118 (2005) 3997–4007.
[23] E. Tzima, M.A. Del Pozo, W.B. Kiosses, S.A. Mohamed, S. Li, S. Chien, M.A. Schwartz, Activation of Rac1 by shear stress in endothelial cells mediates both cytoskeletal reorganization and effects on gene expression, EMBO J. 21 (2002) 6791–6800.
[24] Y. Ueki, N. Sakamoto, T. Ohashi, M. Sato, Morphological responses of vascular endothelial cells induced by local stretch transmitted through intercellular junctions, Exp. Mech. 49 (2009) 125–134.
[25] Y.C. Poh, S. Na, F. Chowdhury, M. Ouyang, Y. Wang, N. Wang, Rapid activation of Rac GTPase in living cells by force is independent of Src, PLoS One 4 (2009) e7886.

BASIC RESEARCH www.jasn.org

SLCO4C1 Transporter Eliminates Uremic Toxins and Attenuates Hypertension and Renal Inflammation

Takafumi Toyohara,* Takehiro Suzuki,* Ryo Morimoto,* Yasutoshi Akiyama,* Tomokazu Souma,* Hiromi O. Shiwaku,* Yoichi Takeuchi,* Eikan Mishima,* Michiaki Abe,* Masayuki Tanemoto,* Satohiro Masuda,† Hiroaki Kawano,‡ Koji Maemura,‡ Masaaki Nakayama,§ Hiroshi Sato,* Tsuyoshi Mikkaichi,‖ Hiroaki Yamaguchi,‖ Shigefumi Fukui,¶ Yoshihiro Fukumoto,¶ Hiroaki Shimokawa,¶ Ken-ichi Inui,† Tetsuya Terasaki,** Junichi Goto,‖ Sadayoshi Ito,* Takanori Hishinuma,†† Isabelle Rubera,‡‡ Michel Tauc,‡‡ Yoshiaki Fujii-Kuriyama,§§ Hikaru Yabuuchi,‖‖ Yoshinori Moriyama,¶¶ Tomoyoshi Soga,*** and Takaaki Abe*†††‡‡‡

*Division of Nephrology, Endocrinology, and Vascular Medicine, §Research Division of Dialysis and Chronic Kidney Disease, ¶Department of Cardiovascular Medicine, and ‡‡‡Department of Clinical Biology and Hormonal Regulation, Tohoku University Graduate School of Medicine, Sendai, Japan; †Department of Pharmacy, Kyoto University Hospital, Faculty of Medicine, Kyoto University, Kyoto, Japan; ‡Department of Cardiovascular Medicine, Nagasaki University School of Medicine, Nagasaki, Japan; ‖Department of Pharmaceutical Sciences, Tohoku University Hospital, Sendai, Japan; **Division of Membrane Transport and Drug Targeting and ††Division of Pharmacotherapy, Graduate School of Pharmaceutical Sciences, Tohoku University, Sendai, Japan; ‡‡CNRS-FRE3093, University of Nice-Sophia Antipolis, Parc Valrose, Nice Cedex 2, France; §§Center for Tsukuba Advanced Research Alliance and Institute of Basic Medical Sciences, University of Tsukuba, Tsukuba, Japan; ‖‖GenoMembrane Inc., Yokohama, Japan; ¶¶Department of Membrane Biochemistry, Okayama University Graduate School of Medicine, Dentistry, and Pharmaceutical Sciences, Okayama, Japan; ***Institute for Advanced Biosciences, Keio University, Tsuruoka, Japan; and †††Division of Medical Science, Tohoku University Graduate School of Biomedical Engineering, Sendai, Japan

ABSTRACT

Hypertension in patients with chronic kidney disease (CKD) strongly associates with cardiovascular events. Among patients with CKD, reducing the accumulation of uremic toxins may protect against the development of hypertension and progression of renal damage, but there are no established therapies to accomplish this. Here, overexpression of human kidney-specific organic anion transporter SLCO4C1 in rat kidney reduced hypertension, cardiomegaly, and inflammation in the setting of renal failure. In addition, SLCO4C1 overexpression decreased plasma levels of the uremic toxins guanidino succinate, asymmetric dimethylarginine, and the newly identified trans-aconitate. We found that xenobiotic responsive element core motifs regulate SLCO4C1 transcription, and various statins, which act as inducers of nuclear aryl hydrocarbon receptors, upregulate SLCO4C1 transcription. Pravastatin, which is cardioprotective, increased the clearance of asymmetric dimethylarginine and trans-aconitate in renal failure. These data suggest that drugs that upregulate SLCO4C1 may have therapeutic potential for patients with CKD.

J Am Soc Nephrol 20: 2546–2555, 2009. doi: 10.1681/ASN.2009070696

Received July 3, 2009. Accepted September 9, 2009.

Published online ahead of print. Publication date available at www.jasn.org.

T.To., T.Su., and R.M. contributed equally to this work.

T.H. is deceased.

Correspondence: Dr. Takaaki Abe, Division of Medical Science, Tohoku University Graduate School of Biomedical Engineering, Sendai 980-8574 Japan. Phone: • 81-22-717-7163; Fax: • 81-22-717-7168; E-mail: takaabe@mail.tains.tohoku.ac.jp; or Dr. Takehiro Suzuki, Division of Nephrology, Endocrinology, and Vascular Medicine, Tohoku University Graduate School of Medicine, 1-1 Seriyo-cho, Aoba-ku, Sendai 980-8574, Japan. Phone: • 81-22-717-7163; Fax: • 81-22-717-7168; E-mail: suzuki2i@mail.tains.tohoku.ac.jp

Copyright • 2009 by the American Society of Nephrology

All individuals with an estimated GFR (eGFR) • 60 ml/min per 1.73 m^2 are defined as having chronic kidney disease (CKD).[1] The prevalence of CKD is now estimated at approximately 10% of the population and will progress to ESRD. In patients with CKD, the accumulation of uremic toxins causes difficulty in controlling BP, impairs renal function, and worsens prognosis.[2,3] So far, more than 110 organic compounds have been identified as uremic toxins.[4] Among these, guanidino compounds, including guanidino succinate (GSA) and asymmetric dimethylarginine (ADMA), are increased in patients with CKD and correlate with prognosis.[3,5] In particular, ADMA, an inhibitor of nitric oxide synthase, is implicated in hypertension, renal damage, cardiac hypertrophy, and cardiovascular events.[6,7] Currently, administration of the oral adsorbent AST-120 is the only therapy to remove uremic toxins in patients with CKD and diabetic nephropathy.[8] Although AST-120 removes indoxyl sulfate, other compounds are not eliminated.[9] Thus, a new approach that addresses this problem is urgently needed.

Recently, we isolated a human kidney-specific organic anion transporting polypeptide (OATP), termed SLCO4C1, and functionally characterized it as a digoxin transporter.[10] The OATP family is involved in the membrane transport of bile acids, conjugated steroids, thyroid hormone, eicosanoids, peptides, cardiac glycosides (digoxin, digitoxin, and ouabain), and numerous drugs.[10] Among these, in the kidney, SLCO4C1 might be a first step of transport pathway of digoxin and various compounds into urine.[10] In renal failure, basolateral SLCO4C1 expression was decreased; however, the expression level of MDR1, a member of the ATP-binding cassette transporter family that mediates the tubular secretion of digoxin at the apical membrane of the proximal tubule cell, was not changed.[10] This reduction of SLCO4C1 in the proximal tubules may be one of the mechanisms of impaired urinary excretion of digoxin and drugs in renal failure.[10] In humans, SLCO4C1 is the only organic anion transporter in the kidney, whereas, in rodent kidney, several oatps exist at the basolateral and apical membrane of the proximal.[10] This species diversity of the OATP family subtypes and the multiple locations in proximal tubules make it difficult to extrapolate from experimental studies of rodents to humans. To overcome this issues, here, we generated a transgenic (TG) rat harboring human SLCO4C1 in rat kidney and clarified physiologic and pathophysiologic roles of human SLCO4C1.

RESULTS

Generation of TG Rat Harboring Human SLCO4C1 in the Kidney

TG rat harboring human SLCO4C1 in the kidney was generated using the proximal tubule–specific promoter[11] (Figure 1, A and B). In addition, to avoid unusual mRNA splicing during overexpression, we mutated three atypical splicing donor-adaptor sites in the coding region of SLCO4C1 without changing the amino acids (Figure 1A). As a result, the human SLCO4C1 mRNA was exclusively expressed in the kidney, especially in the proximal tubules of TG rats (Figure 1C). Immunohistochemical analysis also revealed that human SLCO4C1 protein was strongly detected at the basolateral side of the proximal tubules (Figure 1D).

When renal mass was reduced by five-sixths nephrectomy (Nx), BP was significantly decreased in TG(•)Nx rats compared with non-TG littermate [TG(•)Nx] rats (Figure 2A). This BP reduction was seen in two independently generated lines. In TG(•)Nx rats, cardiac hypertrophy was also significantly reduced (Figure 2B).

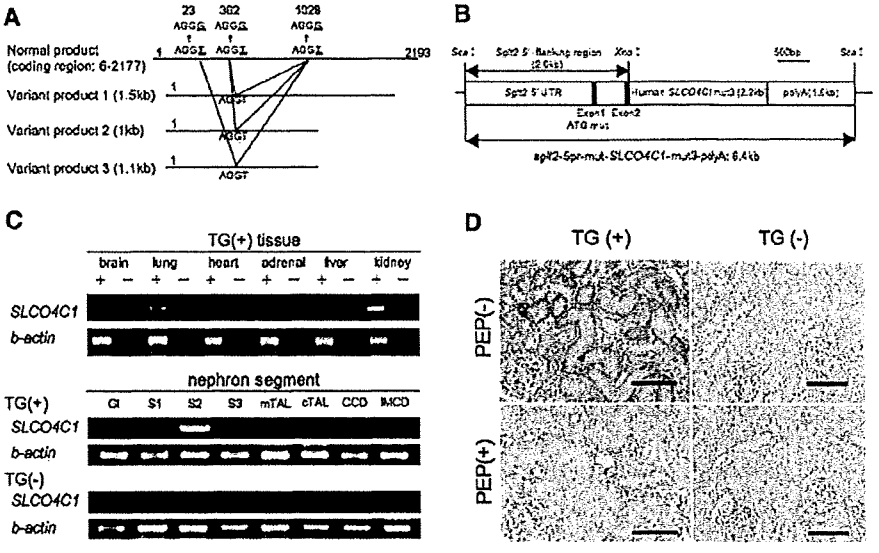

Figure 1. Characterization of human SLCO4C1 TG rats is shown. (A) Three different smaller sizes of mRNA by alternative splicing were found and mutated to avoid unusual splicing (AGGT to AGGG). (B) The mutated human SLCO4C1 cDNA was inserted into a plasmid under the proximal tubule–specific promoter. (C) Expression of human SLCO4C1 in rat organs and microdissected renal tubules examined by reverse transcriptase–PCR. GI, glomerulus; S1, proximal tubule S1 segment; S2, proximal tubule S2 segment; S3, proximal tubule S3 segment; mTAL, medullary thick ascending limb; cTAL, cortical thick ascending limb; CCD, cortical collecting duct; IMCD, inner medulla collecting duct. (D) Immunohistochemical analysis. The human SLCO4C1 immunostains were abolished by peptide absorption. Bars • 100 • m.

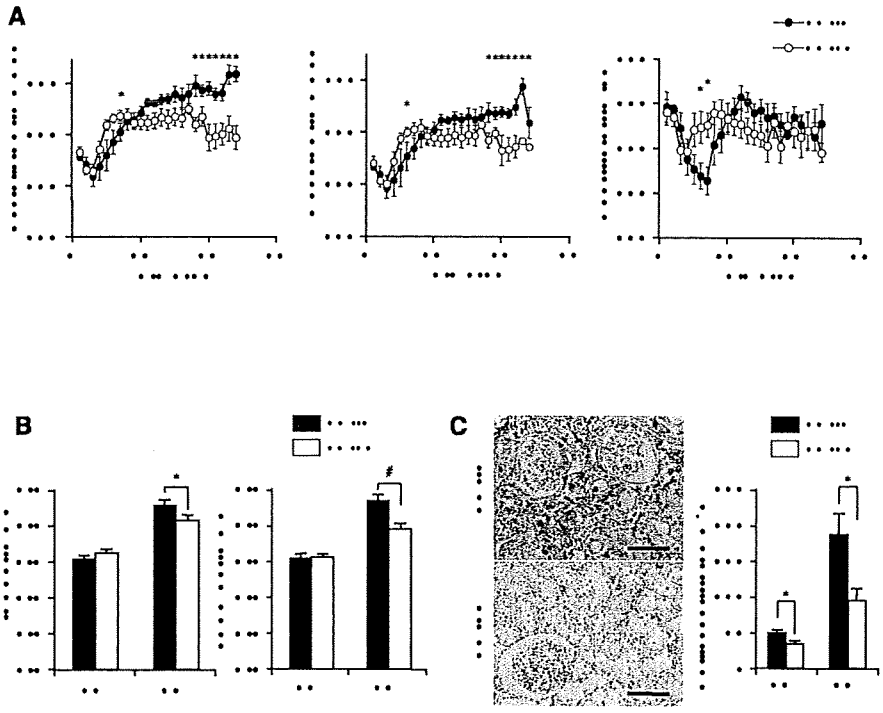

Figure 2. Phenotype of human SLCO4C1 TG rats. (A) BP and heart rate of TG(•)Nx and TG(•)Nx rats. *P • 0.05 versus TG(•)Nx rats (n • 4 to 6 per group). (B) Thickness of the interventricular septum (IVSTd) and left ventricular posterior wall at end-diastole (LVPWTd) were measured by echocardiogram before and 3 wk after five-sixths Nx. *P • 0.05; #P • 0.01 (n • 4 to 9 per group). (C) CD68 staining in the rat kidney before and 3 wk after five-sixths Nx. CD68+ cell number counts were performed before and 3 wk after five-sixths Nx. *P • 0.05 versus TG(•) rats (n • 6 to 9 per group). Bars • 100 • m.

The survival rate of TG(•)Nx rats was slightly increased from that of TG(•)Nx rats, but the results did not reach statistical significance (Supplemental Figure 1C). In patients with CKD, renal inflammation is also a risk factor of renal damage and morbidity and mortality.[12] Immunohistochemically, mononuclear cell infiltration stained with the macrophage marker CD68 was strongly detected in TG(•)Nx rat kidneys (Figure 2C). Conversely, TG(•)Nx kidneys demonstrated less infiltration of macrophage (Figure 2C). These data indicate that expression of human SLCO4C1 in rat kidneys ameliorated not only hypertension but also inflammation in renal failure.

Elimination of Uremic Toxins in TG(•) Rats

To understand the mechanism by which SLCO4C1 exerted antihypertensive and anti-inflammation effects, we performed comprehensive quantitative metabolome analysis.[13] Blood and urine specimens were measured by capillary electrophoresis mass spectrometry (CE-MS) and HPLC, and 188 anions and 298 cations were identified (Supplemental Tables 1 through 4). Among these, we focused on 21 compounds for which concentration was significantly changed after Nx (Supplemental Figure 2). As a result, the plasma levels of creatinine and indoxyl sulfate were increased 3 wk after Nx as previously reported,[4] but the concentrations of these compounds were not different between TG(•)Nx and TG(•)Nx rats 3 wk after Nx (Figure 3, A and B). Conversely, although the plasma concentration of ADMA, GSA, and trans-aconitate were significantly increased 3 wk after Nx, the increments were significantly decreased in TG(•)Nx rats compared with TG(•)Nx rats (Figure 3, C through E). These data suggest the facilitation of the excretion of uremic toxins in TG(•) rats.

To exclude the possibility of the compensative or nonspecific effects by overexpression of SLCO4C1 in the kidney, we performed microarray analysis. As a result, there was NS difference in the expression levels of other rat transporters (slco4c1, oatp1, oatp3, oatp5, abcb11, mrp2, mdr1, and mlc1).

The serum ADMA level is controlled by two pathways: (1) Enzymatic degradation by dimethylarginine dimethylaminohydrolase (DDAH) and (2) urinary excretion.[14] In TG(•)Nx rats, the DDAH1 mRNA level was not different between TG(•)Nx and TG(•)Nx rats, and the DDAH2 mRNA level in TG(•)Nx rats was decreased compared with TG(•)Nx rats (Figure 3F), suggesting that the decrease of ADMA in TG(•)Nx rats was not dependent on facilitating enzymatic degradation. In addition, neither the plasma level of citrulline (Figure 3G), produced from ADMA by DDAHs, nor the mRNA level of protein arginine N-methyltransferase that generates ADMA from arginine was different between TG(•)Nx and TG(•)Nx rats. Because GSA excretion had not completely correlated with creatinine clearance,[15] these data further suggest that the overexpression of SLCO4C1 at the proximal tubule facilitates guanidino compound excretion in renal failure.

Trans-aconitate is a competitive inhibitor of aconitase.[16] Aconitase is a key enzyme in catalyzing citrate to isocitrate via cis-aconitate in the TCA cycle, and the accumulation of trans-aconitate inhibits TCA cycle and respiration in tissues.[16] The retention compounds that are biologically/biochemically active and responsive for the uremic syndrome are called uremic toxins.[4] It is widely known that he accumulation of guanidino compounds (including ADMA and GSA) and several uremic toxins generate oxidative stress, and it causes further renal

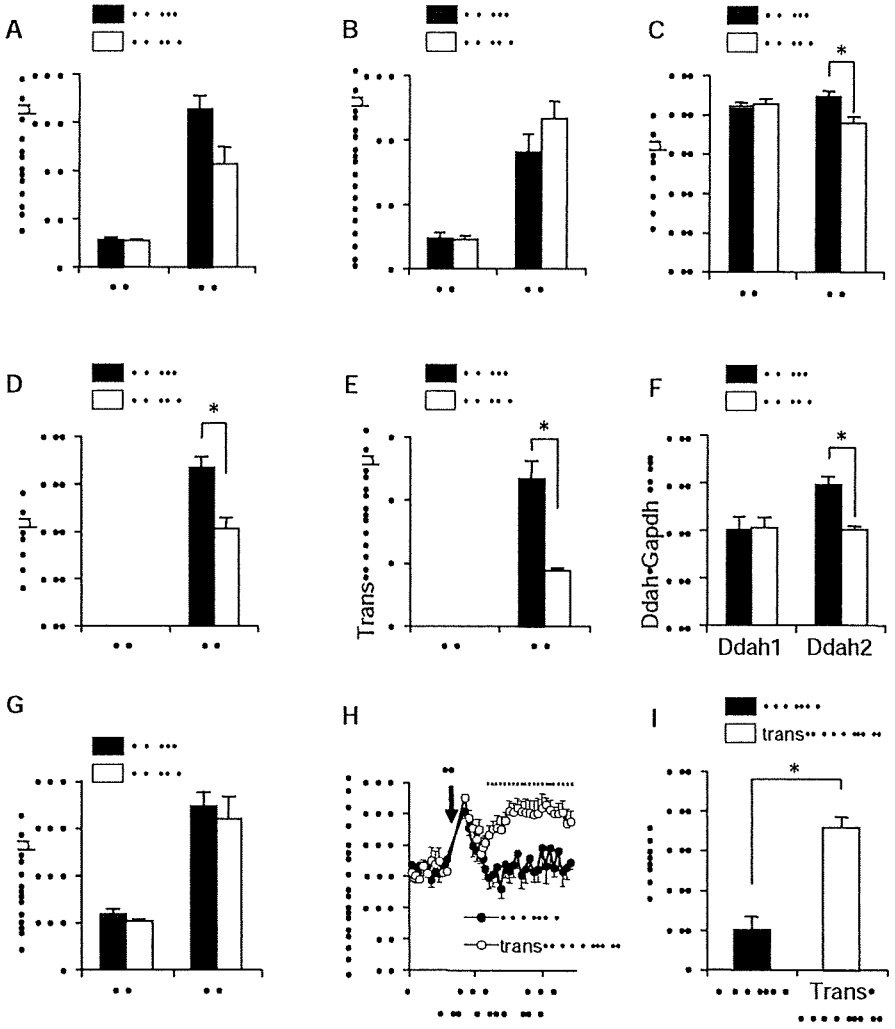

Figure 3. Metabolome analysis and characterization of uremic toxins are shown. (A through E and G) The plasma concentration of creatinine (A), indoxyl sulfate (B), ADMA (C), GSA (D), trans-aconitate (E), and citrulline (G) before and 3 wk after five-sixths Nx (n • 4 to 5 per group). (F) The mRNA expression level of DDAH1 and DDAH2 in the kidney 3 wk after five-sixths Nx (n • 5 per group). (H) BP after intraperitoneal injection of trans-aconitate (400 mg/kg; n • 5 per group). (I) Trans-aconitate–induced superoxide production in HK-2 cells. *P • 0.05.

damage in patients with CKD[17]; however, the existence in mammals, biologic effects, and the precise role of trans-aconitate in renal failure have not been clarified. When trans-aconitate was administered to rats intraperitoneally, the BP of injected rats was immediately elevated compared with controls (Figure 3H). This increase of BP was cancelled when trans-aconitate was injected into TG(•) rats compared with TG(•) rats, further suggesting the excretion through SLCO4C1 (Supplemental Figure 1D). In addition, trans-aconitate significantly induced superoxide production in human kidney proximal tubule cells (Figure 3I).

To confirm further that not only ADMA and GSA but also trans-aconitate exists in humans and the concentration is increased in accordance with CKD progression, we performed CE-MS analysis of 41 patients with CKD at various stage. The plasma level of trans-aconitate was significantly correlated with the increase of plasma creatinine, and that inversely correlated with the eGFR similar to ADMA and GSA (Figure 4). Because the plasma level of trans-aconitate in patients without CKD is low, these data suggest that trans-aconitate can be a new uremic toxin, and a newly identified biomarker for predicting the onset of renal damage and, thus, the elimination of trans-aconitate plays a beneficial role in CKD.

Functional Analysis of SLCO4C1 Promoter and Its Modulation by Statins

We assumed that enhancement of SLCO4C1 in the kidney may facilitate the excretion of uremic toxins and thereby ameliorate the symptoms of CKD. In this scenario, drugs that upregulate SLCO4C1 in the kidney may facilitate excretion of uremic toxins and reduce renal inflammation, decelerating progression of renal damage and entry of hemodialysis. To address this, we isolated the promoter region of human SLCO4C1. Human SLCO4C1 promoter region has a predominant transcription start site located 164 bp upstream of the ATG codon (Figure 5A). Potential cis-acting motifs for GATA-1, hepatocyte nuclear factor (HNF)-3•, CCAAT/enhancer-binding protein (C/EBP)•, C/EBP•, cAMP response element-binding protein (CREB), and peroxisome proliferator–activated receptor • were found. We also identified tandem xenobiotic-responsive element (XRE) motifs containing the substitution-intolerant core sequence 5•-CACGC-3• at position • 126 (GGCACGCCCACGCCG). That sequence is generally recognized by AhR and AhR nuclear translocator heterodimer,[18] although the flanking sequences are not typical compared with cyp1a1 XRE motifs[19,20] (Supplemental Figure 3D). AhR binds "classical" ligands such as the environmental pollutants halogenated aromatic hydrocarbons (e.g., dioxin, benzo[a]pyrene, 3-methylcholanthrene [3-MC]).[21]

Human SLCO4C1 promoter activity was increased 1.49-fold (• 2064) and 1.68-fold (• 129) by 3-MC compared with controls (Figure 5B). The • 129 construct exhibited the highest activity, and this segment contained XRE core motifs. Because AhR can also bind to a structurally divergent range of chemicals,[21] we next screened various compounds. The hepatic hydroxymethyl glutaryl–CoA reductase inhibitor (statin) fluvastatin (2.3-fold at 10 • M) and pravastatin (1.3-fold at 30 • M) and atypical AhR ligand flutamide (1.4-fold at 10 • M) upregulated the SLCO4C1 promoter activity (Figure 5C). Because of the comparable magnitude to 3-MC and its clinical availability, we further focused on statins. Deletion experiments showed that all constructs exerted potent promoter activation, but removal of the XRE core segment or mutation in the XRE core motifs abolished the response to fluvastatin (Figure 5D). Because there are various clinical reports on renoprotective effects of statins,[22] we further examined various statins on human SLCO4C1 transcription. Simvastatin, lovastatin, cerivastatin, itavastatin, mevastatin, atorvastatin, rosuvastatin, and pitavastatin upregulated SLCO4C1 transcription (Figure 5F).

Next, we determined the ligand-dependent recruitment of the AhR-XRE system by chromatin immunoprecipitation (ChIP) assay. Application of the antibody against AhR resulted in a positive band for both 3-MC and fluvastatin (Figure 5E, top). In addition, the nuclear recruitment of AhR protein was further confirmed by Western blotting with a strong band in the nuclear extract by 3-MC and fluvastatin (Figure 5E, bottom). These data suggested that statins regulate SLCO4C1 transcription through the AhR-XRE system.

Statins Increase Tubular Uremic Toxin Excretion

On the basis of our results, we next examined the effect of statins in renal failure. In human kidney proximal cells, application of fluvastatin and pravastatin significantly potentiated the SLCO4C1 mRNA by 1.72- and 1.73-fold, respectively (Figure 6A). The uptake of thyroid hormone T3, a representative ligand of SLCO4C1, was also significantly potentiated by fluvastatin and pravastatin by 1.3- and 1.4-fold, respectively (Figure 6B), suggesting the potentiation of SLCO4C1 function in the proximal tubules.

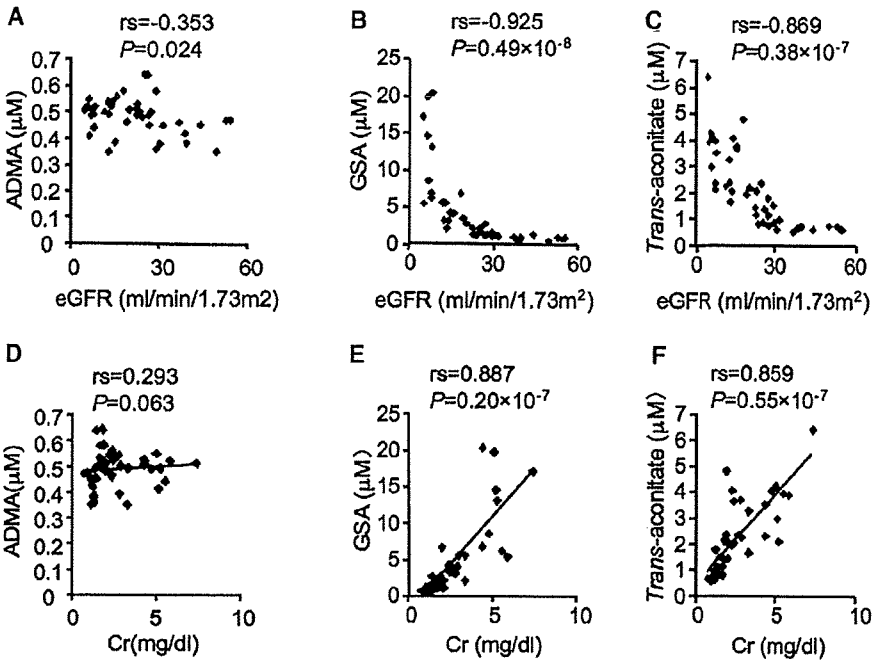

Figure 4. Relation between uremic toxins and eGFR as well as plasma creatinine in 41 patients with CKD is shown. (A through C) Correlations between eGFR and the plasma ADMA (A), GSA (B), and trans-aconitate (C) in patients with CKD. (D through F) Concentrations between plasma creatinine (Cr) and plasma ADMA (D), GSA (E), and trans-aconitate (F).

We next examined the effects of pravastatin in vivo. We and other groups reported that pravastatin reduced BP.[23,24] In addition, pravastatin has been reported to modulate DDAH activity and modulate ADMA concentration.[25] To avoid the effect on BP and to eliminate other pleiotropic effects of pravastatin, we administered low-dosage pravastatin to Nx Wistar rats and examined renal tubular function. After administration of pravastatin, BP was not changed but the mRNA level of rat slco4c1 was significantly increased in the kidney (Figure 7, A and B). Under this condition, the ADMA and trans-aconitate clearance were significantly increased in pravastatin-treated Nx rats without changing creatinine clearance, although the GSA clearance was not statistically significant (Figure 7, C through F). Furthermore, the mRNA level of DDAHs, protein arginine N-methyltransferases, or other transporters was not changed (data not shown). These data strongly suggested that pravastatin increased ADMA and trans-aconitate excretion in the proximal tubules. In addition, cardiac hypertrophy was decreased in the pravastatin-treated group (Figure 7G).

DISCUSSION

Here, we found that the plasma concentration of uremic toxins ADMA, GSA, and trans-aconitate were significantly reduced in

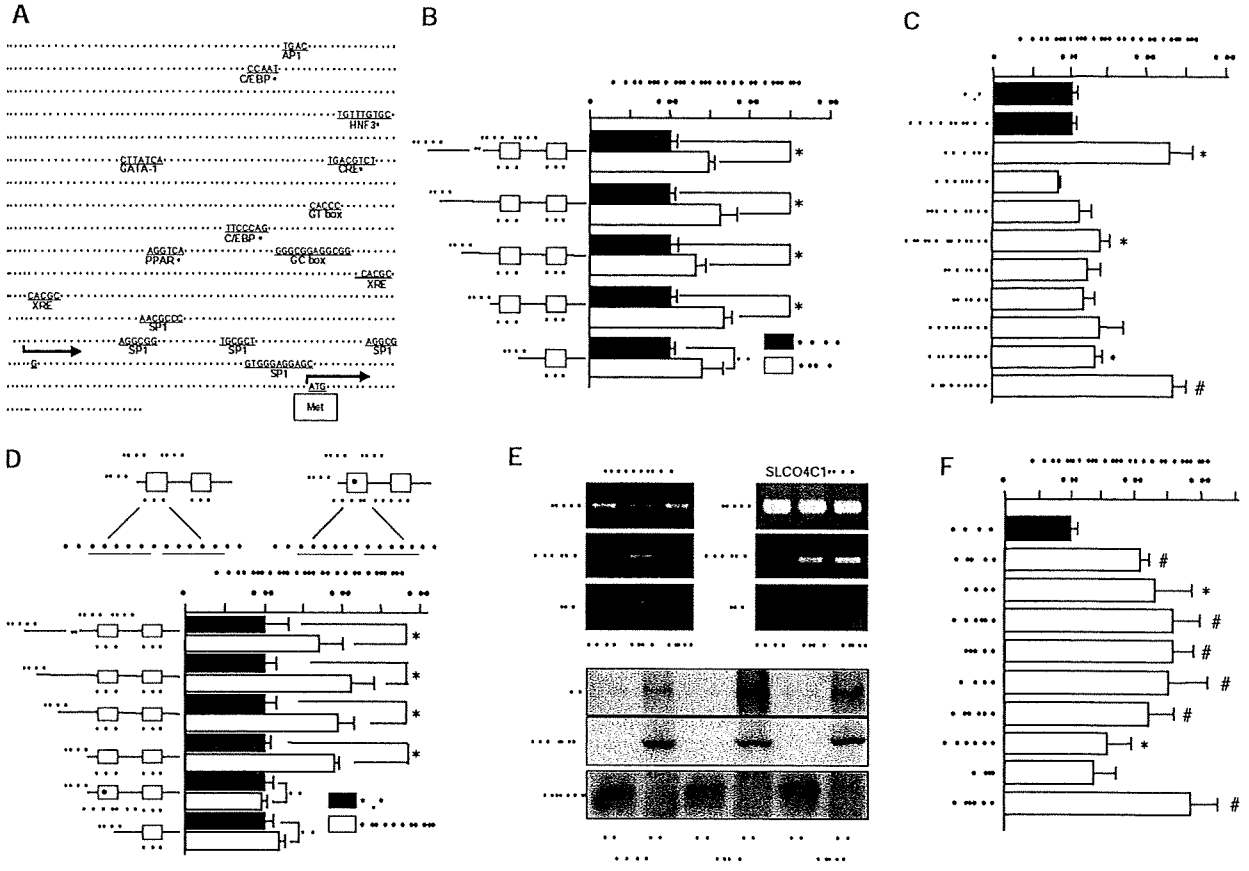

Figure 5. Transcriptional analysis and ligand screening are shown. (A) The 5• region of human SLCO4C1. Potential cis-acting sequences are indicated. Met, first methionine. (B) Promoter activity of human SLCO4C1. Deletion constructs of the human SLCO4C1 promoter region were analyzed with 3-MC (5 • M). *P • 0.05 (n • 3 to 4 per group). (C) Enhancement of promoter activity of human SLCO4C1 with various compounds (concentration as indicated, • M). Quer, quercetin; t-BHQ, tert-butylhydroquinone; I3C, indole-3-carbinole; IS, indoxyl sulfate; Tauro, taurocholic acid; Prava, pravastatin; Fluva, fluvastatin. *P • 0.05 versus DMSO; #P • 0.05 versus H_2O (n • 3 to 4 per group). (D) Effect of fluvastatin (10 • M) on human SLCO4C1 transcription. Deletion constructs and loss-of-function mutation construct in XRE motifs of human SLCO4C1 were examined. *P • 0.05 (n • 3 to 4 per group). (E) ChIP assay and Western blotting of 3-MC or fluvastatin-treated cells. (Top) After application of 3-MC (1 • M) or fluvastatin (10 • M), fixed cell extract was analyzed by mouse cyp1a1 XRE or human SLCO4C1 XRE PCR. (Bottom) Western blotting of nuclear and cytoplasmic fractions from HEK293T cells were stained with antibodies against AhR, Lamin B, or • -tubulin antibodies. Cy, cytosolic fraction; Nu, nuclear fraction. (F) Enhancement of human SLCO4C1 promoter activity with various statins (10 • M) using the minimal promoter region (• 129). *P • 0.05; #P • 0.01 (n • 3 to 4 per group).

TG(•)Nx rats. The guanidino compounds are a large group of structural metabolites of arginine, and the concentrations of GSA and ADMA are markedly increased in renal failure.[2,3] GSA accumulation causes various harmful effects, such as inhibition of platelet aggregation hemolysis and convulsions.[26] Likewise, ADMA is the most specific endogenous compound with inhibitory effects on NO synthesis, and it has also been implicated in the development of hypertension and adverse cardiovascular events.[6,7] Trans-aconitate, known as anti-feedant in brown plant hoppers,[27] is an inhibitor of aconitase and inhibits the TCA cycle[16]; however, its existence in mammals, especially in renal failure, was not previously known. Compounds that inhibit the TCA cycle are "poison." It is also widely known that fluoroacetate is a "suicide" substrate for aconitase. Acute fluoroacetate poisoning in humans mainly affects the central nervous system, cardiovascular system, and kidney, and the biochemical effects include TCA cycle blockade, respiratory failure, and metabolic acidosis and lactate accumulation.[28] Trans-aconitate administration also increased BP and generated oxidative stresses in rats. These data suggest that the overexpression of SLCO4C1 in the renal proximal tubules in TG(•) rats causes the beneficial effect of excretion of harmful uremic toxins such as ADMA, GSA, and trans-aconitate and proposes a new approach to decrease uremic toxins and to reduce the exacerbation of renal function in patients with CKD (Figure 8).

Here we show that statins function as a nuclear receptor ligand recruiting the AhR-XRE system and upregulating SLCO4C1 tran-

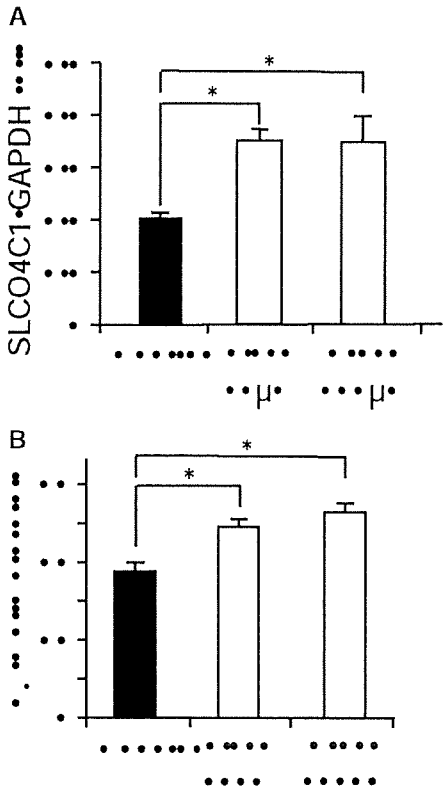

Figure 6. Effects of statins on SLCO4C1 expression and function in vitro. (A) Real-time PCR of SLCO4C1 in ACHN cells with fluvastatin (10 • M) or pravastatin (100 • M; n • 3 per group). (B) The uptake of T_3 by ACHN cells treated with fluvastatin (10 • M) and pravastatin (100 • M). *P • 0.05 (n • 3).

scription to facilitate the excretion of uremic toxins like a transgene phenotype. In patients with CKD, therapy with statins has the potential not only to lower cardiovascular morbidity and mortality but also to slow the progression of renal disease.[22] The effects are thought to be dependent on such mechanisms as a reduction of endothelial dysfunction, inhibition of inflammatory responses, and reduction of oxidative stress.[22,29] Recently, the relationship between statin administration and ADMA was examined in humans. The serum level of ADMA in metabolic syndrome was reduced by fluvastatin.[30] Thus, our data provide new scientific bases for renal protection to facilitate the excretion of uremic toxins in patients with CKD by drugs including statins as "transporter potentiators" (Figure 8). Because the significantly increased levels of GSA and ADMA were reported in patients with autosomal dominant polycystic kidney disease (ADPKD),[5] our data also support the clinical study and will be a new clue for further protection of renal damage in patients with ADPKD.

Cytochrome P-450 (CYP) comprises a superfamily of enzymes that catalyze oxidation of numerous xenobiotic chemicals, including drugs, toxic chemicals, and carcinogens, as well as endobiotic chemicals.[31] Among these CYP enzymes, cyp1a1 is important in the metabolism of carcinogens such as dioxin and halogenated aromatic hydrocarbons.[31] Because of the prominently catalyzing role, it has been believed that compounds that induce cyp1a1 activation are detrimental to humans and animals; however, it is also reported that induction of cyp1a1 is a sensitive but nonspecific indicator of AhR binding and activity, and the induction of cyp1a1 and activation of AhR are not synonymous with dioxin-like toxicity, including carcinogenesis.[32] Clinically, various weak AhR ligands, such as flutamide, omeprazole, and atorvastatin, were identified[32] but the Food and Drug Administration approves usage of these compounds, and in fact, they do not produce dioxin-like toxicities, including carcinogenesis in humans. Because statins have been used for a long time with a high safety and tolerability profile, induction of SLCO4C1 by statins in the kidney in patients with CKD and ADPKD may be a safe and new therapeutic tool to excrete uremic toxins and for reduction of renal inflammation.

We also found that the activation potency of the AhR-XRE system differs between cyp1a1 and slco4c1 in the kidney. In the rat liver, cyp1a1 was significantly induced by flutamide (329-fold) and omeprazole (79-fold), although renal cyp1a1 was weakly upregulated by flutamide (three- fold) and omeprazole (15-fold; Supplemental Figure 3, A and B). It is also reported that some statins significantly induced cyp1a1 in kidney but rather weakly in the liver, suggesting that statins act as AhR ligands mainly in the kidney.[32] Conversely, the renal activation of slco4c1 by flutamide and omeprazole was quite weak (Supplemental Figure 3C). Thus, further exploring for drugs that upregulate human SLCO4C1 only in the kidney much more potently than statins should be a new clinical tool for patients with CKD and ADPKD to decelerate renal damage and to delay initiating hemodialysis.

Metabolomics is an emerging tool that can be used to gain insights into cellular and physiologic responses. By CE-MS, we identified various renal failure–related compounds (Supplemental Figure 2, Supplemental Tables 1 through 4). In renal failure, indoxyl sulfate, creatinine, GSA, and guanidinoacetate were reported as uremic toxins.[4] Increase of citrulline and trimethyl N-oxide,[33] 3-methylhistidine,[34] N,N-dimethylglycine,[35] and allantoin[36] and decrease of carnitine,[37] Trp, and Tyr[38] were also reported in renal failure.

On the other hand, increase of trans-aconitate, 4-acetylbutyrate, hexanoate, argininosuccinate, • -aminoadipate, and pipecolate and decrease of desethylatrazine and methionine sulfoxide so far have not been reported in renal failure (Supplemental Figure 2). Thus, our data will be useful for clarifying the metabolic pathway of renal failure.

CONCISE METHODS

Materials

Pravastatin was provided by Daiichi-Sankyo (Tokyo, Japan). Other statins were purchased from Sequoia Sciences (St. Louis, MO).

Construction of Kidney-Specific TG Rats

The mutated coding region of human SLCO4C1[10] was inserted into the pGEM-sglt2–5pr-mut plasmid containing kidney-specific sglt2 pro-